Identification of Nitric Oxide Synthase Neurons for Laser Capture Microdissection and mRNA Quantification

BioTechniques 33:1274-1283 (December 2002)

Wenya Linda Bi, Christine Keller-McGandy, David G. Standaert, and Sarah J. Augood
Massachusetts General Hospital, Charlestown, MA, USA

ABSTRACT

An immunohistochemical technique was developed to visualize nitric oxide synthase (NOS)-immunopositive neurons in fresh-frozen tissue sections of rat brain for laser capture microdissection (LCM) and mRNA analysis. The effect of tissue fixation and the choice of fluorophore were investigated. Here we describe a rapid immunofluorescence protocol that allows the processing of fresh-frozen tissue sections within eight minutes and subsequent mRNA extraction and real-time PCR from pools of 20 NOS-immunopositive LCM neurons. The cellular complement of a subset of ionotropic glutamate receptors, specifically N-methyl-D-aspartate receptor subunit mRNAs, was examined because these receptor complexes are thought to mediate the effects of fast and slow glutamate excitotoxicity. Real-time PCR data revealed that striatal NOS interneurons express the mRNAs encoding NR1, NR2A, NR2B, and NR2D but not NR2C. These LCM mRNA data are consistent with previous in situ hybridization studies and demonstrate the utility of rapid immuno-LCM with real-time quantitative PCR for the study of mRNA abundance in discrete populations of neurons within the mammalian brain.

INTRODUCTION

Measurements of mRNA abundance are powerful analytical approaches to the study of cell physiology and the effects of disease state on cell function. Indeed, numerous studies have identified abnormalities in specific transcriptional pathways that may underlie the pathophysiology of several disease processes (1,9,21,26,29,31). Recent technological advances, in particular the development of rapid quantitative methods for PCR coupled with focused gene array technologies, have greatly extended the usefulness of mRNA profiling.

In neurobiological research, an important consideration is the very high degree of cellular heterogeneity present in the brain. With conventional dissection techniques, it is inevitable that tissue samples from the brain will contain a variety of different cell types, both neuronal and glial, confounding data interpretation. Anatomical techniques such as in situ hybridization are often used to circumvent this problem, but this approach is limited to the study of one or two genes at a time, and quantitation is laborious (28). Laser capture microdissection (LCM) is a method for the harvesting of single cells from heterogeneous tissue sections (12,37). Originally developed for studies of cancer, LCM is currently being used by several laboratories to isolate populations of neurons from the brain for mRNA profiling (6).

The application of LCM for mRNA profiling in the central nervous system presents several significant technical challenges. Different LCM systems are currently available (44), and the physical extrication of the cell from the tissue section depends on several parameters, including the thickness of the section, method of tissue fixation, and coating of the microscope slide that the tissue is mounted on. Many general histological staining protocols have been successfully modified for use with LCM, including hematoxylin and eosin, methylene blue, and methyl green (38). In contrast, the neurochemical identification and capture of specific populations of neurons have proved more difficult. We have found the use of histochemical reactions such as NADPH-diaphorase problematic, as the protocols require incubation of the tissue section at 37°C, which results in irreversible binding of the tissue to the microscope slide. Further, the presence of metal ions, which are often integral components of many histological protocols, can also have a negative effect on RNA recovery.

Routine immunohistochemical techniques are generally not compatible with subsequent RNA analysis because they require long incubation times in aqueous solutions, conditions in which mRNA is unstable and becomes degraded. However, such limitations may not apply to tissues being processed for DNA analysis or proteomic profiling (25,37,45) where different parameters must be optimized for successful biomolecular recovery. In addition, many routine immunohistochemical protocols require fixation with aldehydes, which may reduce the recovery of mRNA (11,20,22). The chromogen used for immunohistochemical staining must also be selected carefully. Fluorescence is a very sensitive detection

method, but many standard fluorophores are not compatible with LCM because their fluorescence is quenched by dehydration through xylene, a step that is required for successful capture.

We have developed a technique of rapid immunohistochemistry to visualize populations of nitric oxide synthase (NOS)-immunopositive neurons in the rat striatum that is compatible with LCM and subsequent quantitative mRNA analysis. Our interest in this cell population arises from their resistance to neurodegenerative injury. For example, in Huntington's disease, there is an extensive loss of neurons from the striatum, but the NOS-containing population is relatively preserved (10,14,15). Further, striatal NOS interneurons are similarly resistant to both chronic and acute ischemia, hypoxic trauma (32–34), mitochondrial toxins (7,23), and excitotoxins (3–5). In these initial studies, we have used real-time PCR to analyze the expression of the mRNAs encoding members of the family of ionotropic glutamate receptors, specifically N-methyl-D-aspartate (NMDA) receptors; these receptor complexes are a key component of the excitotoxic cascade. We have found that this rapid immunofluorescence method provides an effective and efficient strategy for isolating mRNA from a neurochemically identified population of neurons. This approach should be readily extendable to studies of other cell types and types of mRNA analysis, including gene array profiling (6).

MATERIALS AND METHODS

Rat Tissue

Adult Sprague-Dawley rats were obtained from Charles River Laboratories (Wilmington, MA, USA). Their brains were removed and immediately snap-frozen in ice-cold isopentane. Frozen brain tissue was then mounted onto a cryostat chuck, and 8-µm-thick fresh-frozen tissue sections were cut and thaw-mounted onto RNase-free uncoated, uncharged microscope slides (Fisher Scientific, Pittsburgh, PA, USA). Coronal sections were cut from three adult rat brains and stored at -80°C until processed for LCM.

Optimization of Tissue Preparation for LCM

We examined in detail both the effects of fixation and the choice of fluorophore on the identification of NOS neurons in the rat striatum. NOS immunostaining was carried out by incubating the frozen tissue section in fixative, rinsing briefly (1 min) in 100 mM sodium phosphate buffer, pH 7.4, followed by incubation in primary rabbit anti-nNOS antiserum (Sigma, St. Louis, MO, USA) diluted 1:500 in 100 mM phosphate buffer for 5 min, another brief rinse in phophate buffer, incubation in goat-anti-rabbit IgG (diluted 1:50 in 100 mM phosphate buffer; Molecular Probes, Eugene, OR, USA), and rinse and rapid dehydration (70%, 80%, 95%, 100% ethyl alcohol) to xylene. In optimizing the protocol, we tested both paraformaldehyde in 100 mM phosphate buffer, pH 7.4, at various concentrations (0.5%, 1%, 2%, and 4%) and ethanol (70%, 80%, 90%, and 100%) as a fixative. The duration of fixation was varied from 30 s to 5 min. We tested a variety of different fluorophores, including the cyanine dyes (Cy2 and Cy3), tetramethylrhodamine (TRITC) (Jackson ImmunoResearch Laboratories, West Grove, PA, USA), and Alexa Fluor 488 (Molecular Probes). We also examined the effect of varying the concentration and incubation time of the primary anti-NOS antiserum and the effect of xylene dehydration on the abundance and intensity of cellular staining. To compare the effects of these variables, we prepared sections stained under different conditions and evaluated both the abundance and intensity of immunofluorescent NOS interneurons detected both before and after xylene dehydration. Immunopositive cell bodies observed were counted and compared to adjacent sections processed for NADPH-diaphorase histochemistry, an established histochemical marker of NOS interneurons (43). NADPH-diaphorase histochemistry was carried out as previously described (36).

LCM Dissection

NOS-immunopositive striatal interneurons were laser dissected (PixCell II®) and collected on HS CapSure™ caps (both from Arcturus, Mountain View, CA, USA). The laser pulse settings were 30–50 mW, with a duration of 1.2–1.5 ms as previously described (30). For the quantitative PCR studies, 200 NOS-immunopositive striatal neurons were dissected from each rat striata.

RNA Extraction, DNase Treatment, and First-Strand DNA Synthesis

Total RNA was extracted from LCM neurons using a Micro RNA isolation Kit (Stratagene, La Jolla, CA, USA), per the manufacturer's instructions. In brief, CapSure polymer caps were attached to sterile 0.5 mL Eppendorf® tubes containing RNA extraction buffer (200 µL guanidinium isothiocyanate and 1.6 µL β-mercaptoethanol), the tubes inverted on ice for 15 min, centrifuged, processed immediately, or stored at -80°C. To the extraction buffer, 20 µL sodium acetate (2 M), 200 µL phenol (pH 5.2), and 60 µL chloroform-isoamyl alcohol were added, the sample vortex-mixed, placed on ice for 15 min, and centrifuged at 4°C for 15 min. The upper aqueous layer was then transferred to a new Eppendorf tube, and 2 µL glycogen (10 mg/mL; GenHunter, Nashville, TN, USA) and 200 µL ice-cold isopropanol were added, the RNA was precipitated at -80°C and then recovered by centrifugation at 4°C. The RNA pellet was then rinsed, re-centrifuged, and resuspended in DNase buffer (MessageClean Kit, GenHunter) containing RNase inhibitor (20 U) and DNase I (20 U), and incubated at 37°C for 2 h to eliminate contaminating genomic DNA. First-strand DNA synthesis was then carried out using 50 U SuperScript® II (SuperScript II Preamplification Kit; Invitrogen, Carlsbad, CA, USA) at 42°C for 50 min.

PCR Primers

Short synthetic (20-mer) primers were designed using the Oligo® 4.0 program (Molecular Biology Insights, Cascade, CO, USA) to generate 100–300 bp PCR products. Primer sets were designed to amplify the products for the NMDA receptor subunits NR1,

Table 1. PCR Primer Sets Used for Real-Time PCR of LCM Striatal Neurons

Primers	Sequence (5′→3′, Forward/Reverse)	Nucleotides Product Size	GenBank® Accession No.	Reference No.
SOM	AAACAGGAACTGGCCAA/ TGTCTTCCAGAAGAAGT	193–396 (203 bp)	M25890	(28)
ENK	ACAACCGTGCGAAAGATAGC/ TGATAGTCCATCCACCACTC	542–735 (193 bp)	M28263	(41)
NF-*l*	CAAGAACACCGACGCAGTGC/ TTCGCCTTCCAAGAGTTTCC	950–1263 (313 bp)	AF031880	in-house
GFAP	CTGCCAGGGTAGACTTCT/ CCTTGTTTTGCTGTTCCA	139–294 (155 bp)	J04569	in-house
IT15	GCTCATTCCAGTTGTTAGTG/ GGTAGTTTTCCATCAGGTAG	8348–8476 (128 bp)	U18650	(18)
NR1	CGACACGGCTCTTGGAAG/ TAGGCGGGTGGCTAACTA	419–555 (136 bp)	X63255	(39)
NR2A	CGCCAGGATTCTCTAAACCA/ CGGTCAACATCGCTACAGTC	3079–3304 (225 bp)	D13211	(39)
NR2B	AGCCAAGAGGAGGAAACAGC/ ACCTCCACTGACCGAATCTC	3288–3568 (280 bp)	M91562	(39)
NR2C	CGAGAACTGGGGCAACAACC/ GGGACACATCGGGCAAAGGT	3161–3358 (197 bp)	D13212	(39)
NR2D	CTTCTCCGTCCCCTTTGTAG/ CAGCAGCCAGATGGATTTCC	1677–1933 (256 bp)	D13213	(39)

Eight of the specific primers used were modified from previously published sequences. GFAP and NF-*l* were designed and synthesized in-house.

NR2A, NR2B, NR2C, and NR2D, the Huntington's disease gene IT15, the neuropeptides somatostatin (SOM) and enkephalin (ENK), neurofilament-light (NF-*l*), and glial fibrillary acidic protein (GFAP; an astrocyte marker). The NR1 primer set was designed to amplify all NR1 splice variants. Eight of the 10 primer sets are modifications of previously published sequences (Table 1). To evaluate the relative abundance of each transcript across samples, a real-time PCR protocol was optimized so that all 10 primer sets could be assayed in parallel, at the same annealing temperature in a 96-well plate (iCycler, Bio-Rad Laboratories, Hercules, CA, USA), with SYBR® Green I dye as the fluorogenic marker. The use of SYBR Green obviates the need for target-specific fluorescent probes; however, its specificity is determined entirely by the primers and efficiency of PCR (8).

Optimization of the PCR Protocol

To evaluate the relative abundance of each transcript across samples, it was critical to optimize the PCR so that all samples could be assayed in parallel, at the same annealing temperature. The predicted optimal annealing temperatures for these primer sets ranged from 50.3°C to 58°C, except for NR2C, which was relatively higher (63.8°C) due to the mRNA sequence being GC rich. We determined empirically the PCR efficiency of each of the primer pairs at annealing temperatures between 56°C and 58°C. The PCR efficiency was calculated according to Equation 1 and is expressed as a percentage of a theoretical ideal efficiency, doubling the DNA PCR product with each polymerization cycle (24).

$$\text{PCR efficiency} = (\text{actual amplification rate}/2) \times 100 \quad \text{[Eq. 1]}$$

$$\text{Actual amplification rate} = \exp.[\text{slope of linear log (RFU)}] \quad \text{[Eq. 2]}$$

RFU = relative fluorescent unit

To determine the lower limit of cDNA required for efficient real-time PCR, dilutions were prepared from mRNA isolated from 1000 striatal neurons, visualized by methylene blue histochemistry. Aliquots containing 100, 25, and 6.25 LCM neuron equivalents were processed for real-time PCR using the ENK PCR primer set.

Real-Time PCR

Real-time PCR was carried out in a 96-well plate using an iCycler and a premade SYBR Green PCR Master Mix (Applied Biosystems, Foster City, CA, USA). The Master Mix consists of SYBR Green I dye, AmpliTaq Gold® DNA polymerase (27), $MgCl_2$, dNTP mixture, and other proprietary components. The final reaction volume contained 50 µL comprising primers (500–300 nM), cDNA, and Master Mix. Each of the three DNA samples generated from 200 LCM striatal neurons was divided into 10 aliquots (corresponding to 20 NOS neuron equivalents) and used for real-time PCR. Thus, for each sample of NOS-immunopositive neurons, 10 samples were generated and each sample was processed for real-time PCR using one of the 10 primer sets. All samples from each of the three rats were pro-

Table 2. Effect of Tissue Fixation and Duration on the Intensity and Abundance of NOS Neurons in the Rat Striatum

Fixative/Time	30 s	1 min	3 min	5 min
4% PFA	——	* * / ++	* * * / ++	* * * / +++
2% PFA	* * / ++	* * * / +++	* * * / +++	* * * / +++
1% PFA	* / +	* / + +	——	——
0.5% PFA	——	* / +	——	——
100% EtOH	——	——	——	* * * / +++
90% EtOH	——	——	* * / ++	* * / +++
80% EtOH	* * / ++	* * * / +++	* * * / +++	——
70% EtOH	——	——	* * / ++	– / –

Abundance of neurons: +++, high; ++, moderate; +, low; –, none observed. Dotted lines, not tested.
Signal intensity: ***, high; **, moderate; *, weak, -, no signal observed. PFA, paraformaldehyde.

cessed simultaneously in the same 96-well plate at an annealing temperature of 56°C. A positive (rat brain cDNA) and negative (water) PCR was run simultaneously; for each experiment a total of 50 samples were run in parallel. Each PCR run consisted of 50 cycles: denaturation at 94°C for 30 s, annealing at 56°C for 1 min, and polymerization at 72°C for 90 s. Finally, the products were maintained at 4°C until the melting curve analysis was performed.

Verification of PCR Products

The identity of the 10 PCR products was evaluated by (*i*) melting curve analysis, (*ii*) ethidium bromide gel electrophoresis, (*iii*) DNA chip analysis (2100 Bioanalyzer; Agilent Technologies, Palo Alto, CA, USA), and (*iv*) direct sequencing. Upon completion of PCR, melting curve analysis was performed in the iCycler. The reaction is heated to 95°C (1 min), and then cooled to 55°C in 0.5°C increments, and the SYBR Green fluorescence was then monitored and plotted against temperature. Specific 200-bp PCR products have a melting temperature in the range of 80°C–86°C, while nonspecific primer-dimers have a melting temperature in the range 68°C–78°C.

PCR products (5 µL) were further resolved by routine ethidium bromide gel electrophoresis in a 1.2% agarose gel and by microcapillary electrophoresis using a DNA 500 LabChip. Finally, SYBR Green PCR products were purified using QIAquick™ PCR Purification Kit to remove contaminating DNA primers and submitted for direct sequencing to the Massachusetts General Hospital (MGH) Sequencing Core facility. The specificity of the sequence data was verified using a BLAST search (National Center for Biotechnology Information).

Real-time PCR Data Analysis

A threshold value approach was used to compare the signals from the real-time PCR of each product. The threshold for detection was defined as the cycle number when the intensity of the SYBR Green fluorescence exceeded 10× the standard deviation of baseline fluorescence. For these experiments, the PCR baseline was determined as the mean fluorescence during cycles 4–15. This PCR baseline was then subtracted from each sample in the 96-well plate, and a threshold value was computed. This threshold assignment algorithm is a component of the iCycler software and is consistent with other real-time PCR studies (24,42). All data were normalized to NF-*l* (17), a neuron-specific marker used in previous PCR studies (24,42).

RESULTS

Development of the Rapid NOS Immunostaining Protocol

One of the most critical steps in obtaining a robust immunosignal using the

rapid protocol was the choice of primary antiserum. We tested several anti-NOS antisera and found the polyclonal N-7155 (1:500; Sigma) to give the most specific and robust staining. When optimizing the rapid immunostaining protocol, we found that a 10- to 100-fold increase in routine antibody concentration often facilitated a positive signal within 5 min. In addition, the effect of tissue fixation on the abundance and intensity of NOS-immunopositive striatal interneurons was also assessed. Both aldehyde and ethanol fixation yielded a positive signal (Table 2). Since the intensity of staining was equivalent, and prior studies have shown better morphological tissue preservation with 80% ethanol compared to 95% ethanol (22) and that aldehyde fixation can impair mRNA recovery (22), 80% ethanol fixation for 1 min was chosen for all subsequent experiments. We found that xylene treatment (twice for 5 min) had a substantial effect on the intensity of the fluorescent staining obtained. Cy2, Cy3, TRITC, and Alexa Fluor 488 all produced strong staining, but only Cy3 and TRITC were unaffected by xylene exposure. The number of detectable striatal NOS-immunopositive interneurons per mm^2 before and after xylene treatment was 8.90 ± 0.62 and 8.03 ± 1.21 for Cy3; 8.64 ± 0.17 and 7.15 for TRITC; and 5.79 ± 1.26 and 4.34 ± 1.70 for NADPH-diaphorase histochemistry. Thus, for all subsequent NOS immunostaining, Cy3-conjugated IgG was used (Figure 1A). Table 3 lists the final rapid immunofluorescence protocol.

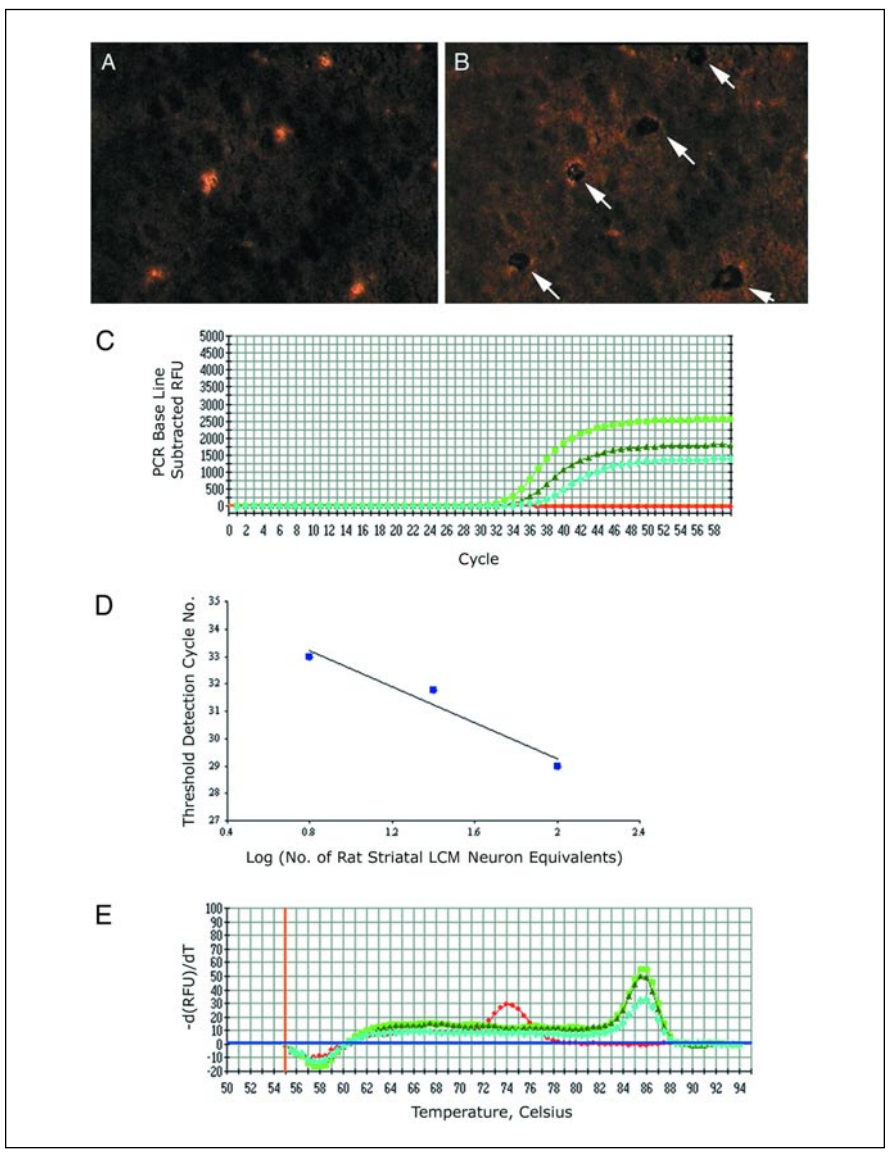

Figure 1. Photomicrographs of five nNOS-immunofluorescent interneurons in the rat striatum before (A) and after (B) LCM. The fluorescence images are of a fresh-frozen section of rat striatum processed for rapid nNOS immunofluorescence and then dehydrated through ethanol and xylene. Images are captured from a dehydrated section with no coverslip. (C) Real-time PCR trace of ENK mRNA abundance in 100 (neon green), 25 (dark green), and 6.25 (aqua) rat striatal LCM neuron equivalents. Note that the threshold cycle number increases with decreasing numbers of cells. No specific signal is observed with the negative control with no DNA (red). (D) Plot of $\log_{10}$ (threshold cycle number) versus relative fluorescence signal for the PCR traces illustrated in panel C. Note the linear ($R^2 = 0.95$) relationship between the detection of the PCR product and the number of LCM neuron equivalents. (E) Melting curve analysis for the PCR trace in panel C. Note that a single peak is observed for each sample derived from 100 (neon green), 25 (dark green), and 6.25 (aqua) LCM neuron equivalents, indicative of a single PCR product with a T_m of approximately 86°C, as expected for the ENK product. By contrast, a primer-dimer complex is observed for the negative control with no DNA (red), which has a T_m of approximately 74°C. RFU, relative fluorescence units.

Table 3. Rapid Anti-NOS Immunofluorescence Protocol

Step	Procedure	Time
1	5–8 µm fresh-frozen section	Thaw 10 s
2	Fix in 80% ethyl alcohol	30–40 s
3	Rinse with 100 mM phosphate buffer, pH 7.4	10 s
4	Incubate in anti-nNOS antiserum, diluted 1:500 in phosphate buffer	5 min
5	Rinse with 100 mM phosphate buffer, pH 7.4	30–60 s
6	Incubate Cy3-anti-rabbit IgG, diluted 1:50 in phosphate buffer	3–5 min
7	Rinse with 100 mM phosphate buffer, pH 7.4	30–60 s
8	Dehydrate through 50%, 70%, 95%, and 100% ethyl alcohol	5–10 s each
9	Xylene	Twice for 5 min

All reagents must be RNase-free or diluted with DEPC-treated water.

Optimization of Real-Time PCR Protocol

The PCR efficiency, as assessed by the slope of the amplification curve (see Materials and Methods section) of each of the 10 primer sets, was evaluated at 56°C and found to be greater than 90% for nine of the 10 primer sets (Table 4). GFAP had an efficiency of amplification of 82% at this annealing temperature.

Data plots of PCR threshold number (Ct) versus log number of LCM neuron equivalents (Figure 1D) revealed a linear correlation coefficient of 0.95, demonstrating that RNA extracted from as few as six striatal neuron equivalents was sufficient for real-time PCR analysis using SYBR Green I dye detection. These findings are in good accord with previous single-cell PCR studies (19,41).

Verification of PCR Products

All 10 primer sets generated a single PCR product of the expected size using control rat brain cDNA as template. However, a specific PCR product was not observed for GFAP and NR2C when using cDNA from laser-dissected NOS neurons, consistent with the absence of expression of these two mRNAs in striatal NOS-immunopositive interneurons. PCR products were assayed by ethidium bromide gel electrophoresis (Figure 2) and by DNA microcapillary electrophoresis (DNA 500 Chip, Bioanalyzer) (Figure 3). In addition, the identity of each product was verified by direct sequencing (MGH DNA Sequencing Core Facility).

Real-Time PCR of Striatal NOS Interneurons

Using the optimal immunostaining protocol, we isolated 200 NOS neurons from sections from three different rats and compared the abundance of the 10 mRNAs in each of the samples. In addition to the DNase treatment of all samples, some were processed in the absence of reverse transcriptase. A PCR product was not observed for any of these samples, which further demonstrates the absence of contaminating genomic DNA (data not shown). Table 4 shows the threshold values (Ct) for each of the 10 primer sets for each replicate. All data are normalized to NF-*l* to allow for inter-assay and intra-assay comparisons. Threshold cycle values greater than 45 were considered nonspecific because of the lack of detectable PCR products by either ethidium bromide gel electrophoresis (Figure 2) or by DNA microcapillary electrophoresis (Figure

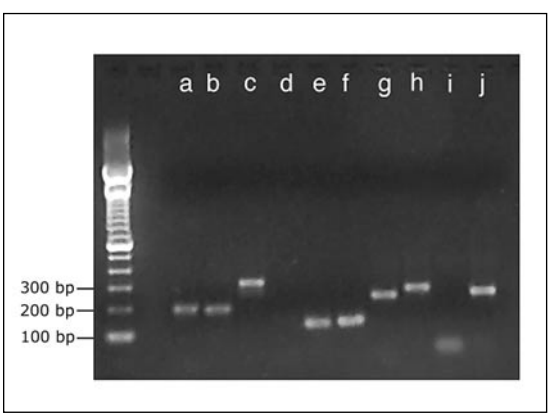

Figure 2. Ethidium bromide gel electrophoresis of the 10 PCR products (a–j) generated from 20 LCM NOS-immunopositive neuron equivalents. All 10 reactions were performed in parallel in the same 96-well plate with an annealing temperature of 56°C. In eight of the 10 samples, a single PCR product of the predicted size was detected. (a) SOM, (b) ENK, (c) NF-*l*, (d) GFAP, (e) IT15, (f) NR1, (g) NR2A, (h) NR2B, (i) NR2C, and (j) NR2D. Note the absence of a specific PCR product in lanes d (GFAP) and i (NR2C).

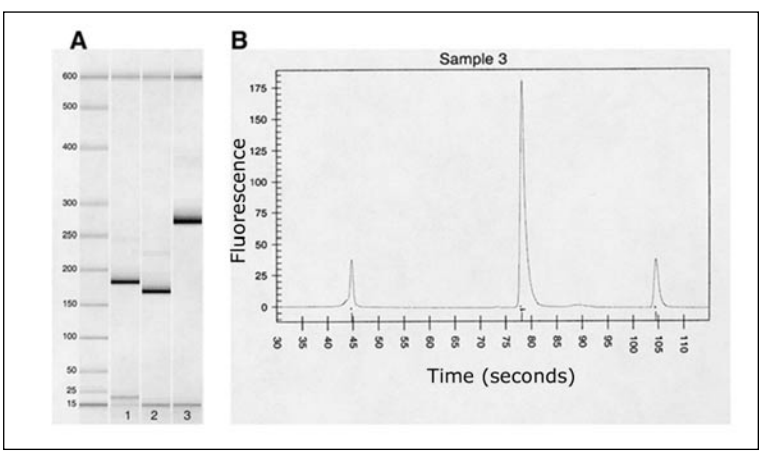

Figure 3. DNA microcapillary electrophoretograms (DNA 500 LabChip, Agilent 2100 Bioanalyzer) of the PCR products generated from laser-dissected NOS-immunopositive neurons. (A) DNA trace of three of the real-time PCR products (lane 1, SOM; lane 2, ENK; and 3, NF-*l*) illustrated in Figure 2. Note that in all three lanes, a single DNA band is detected, which is consistent with the ethidium bromide gel electrophoretogram. (B) DNA spectra of sample 3 (NF-*l*) illustrating the amplification of a single PCR product, which demonstrates the specificity of the SYBR Green PCR method. The minor peaks at approximately 45 and 105 s are internal control spikes present in the sample buffer and used to align the DNA traces.

Table 4. Real-Time PCR Threshold Values for NOS-Immunopositive Interneurons Laser-Dissected from Rat Striata

mRNA:	PCR Efficiency %	A NOS (A)	B NOS (B)	C NOS (C)	D NF-*l* Equivalents $K \times 1.E^{(CtNF-CtX)}$
SOM	99.7	22.41	22.16	20.46	22,859 ± 7.57
ENK	92.5	32.24	36.00	33.81	3.78 ± 1.38
NF-*l*	95.2	35.11	37.16	35.31	1.0
GFAP	81.7	n.d.	n.d.	n.d.	n.d.
IT15	94.4	36.77	39.36	38.33	0.23 ± 0.10
NR1	92.5	30.25	31.30	29.78	35.92 ± 11.28
NR2A	98.8	36.28	37.57	35.64	0.66 ± 0.19
NR2B	91.7	37.18	35.77	36.47	1.03 ± 1.16
NR2C	96.9	n.d.	n.d.	n.d.	————
NR2D	90.2	36.72	37.85	37.97	0.59 ± 0.22

NOS-immunopositive interneurons were simultaneously processed for real-time PCR using 10 primer sets and an annealing temperature of 56°C. (A–C) Values are threshold cycle numbers (Ct) for each of the three independent replicates. n.d., not detected. (D) Data are normalized to NF-*l* (17) and expressed as NF-*l* mRNA equivalents ± SEM.

3). For each replicate, a specific PCR product was obtained for eight of the 10 primer sets; GFAP and NR2C were not detected. The variance of replicates for the normalized threshold cycles was less than 3% for each product. As expected, SOM mRNA was readily detected in this sample of NOS-immunopositive interneurons (threshold, 21.68 ± 1.06). By contrast, the threshold cycle for the detection of IT15 mRNA was 38.16 ± 1.30, suggesting very low levels of expression in this neuron population, consistent with previous PCR data (29). Normalization of the data to NF-*l* mRNA equivalents revealed a relative rank order of threshold cycles for the other five mRNAs as NR1, ENK greater than NR2A, NR2B, and NR2D (Table 4). NR2A, NR2B, and NR2D were detected more than 10 cycles later than SOM mRNA, demonstrating the limited expression of these mRNAs by NOS-immunopositive interneurons.

DISCUSSION

The immuno-LCM protocol described here permits the dissection of a chemically discrete population of NOS-immunopositive neurons from a heterogeneous fresh-frozen tissue section. Further, the protocol has been optimized for the rapid detection of this cell type, permitting the recovery of intact mRNA for subsequent quantitative RNA analysis, specifically real-time PCR. We have demonstrated that the real-time PCR protocol is linear over a range of laser-dissected neuron equivalents and that sufficient intact mRNA can be extracted, reverse transcribed, and used for real-time PCR from as few as 20 neurons. This rapid immuno-LCM protocol can be used to detect NOS-immunopositive neurons in other brain regions, including the cerebral cortex and septum. This protocol can similarly be used to identify NOS-immunopositive neurons for DNA extraction and subsequent direct PCR analysis (data not shown) and in frozen tissue sections from wild-type and transgenic Huntington's disease mouse brain (data not shown) and will facilitate the identification of cell-type-specific "signature" mRNA profiles (6). This rapid protocol adds to those previously described for the identification of specific cell types in complex peripheral tissues (13,16).

Comparisons of expression levels across different mRNAs within any assay is problematic because there are several variables that can impact the data set generated; this is equally true for real-time PCR (8). PCR efficiency is particularly critical. We attempted to minimize the impact of this effect by optimizing our protocol to yield PCR efficiencies greater than 90%. In addition, the method of fluorescence detection can affect data output. We employed a high-throughput protocol using SYBR Green fluorescence detection and monitored the specificity of the PCR-generated product by melting curve analysis, ethidium bromide gel electrophoresis, DNA microcapillary electrophoresis, and direct sequencing. Using these four methods, we are confident that the fluorescent signal generated for each sample is directly attributable to the specific PCR product generated and not to secondary amplifications or primer-dimer complexes.

Given the sensitivity of striatal neurons to the deleterious effects of NMDA receptor agonists and metabolic dysfunction, the complement of NMDA receptor subunits in various types of striatal neurons has been examined previously by single-cell PCR (19) and by dual-label in situ hybridization (2,39), providing a reference platform for the development of the current protocol. In general, data from these two experimental approaches were concordant and differed only in their relative cellular expression of NR2A and NR2B. Using single cell PCR, there appears to be a relative enrichment of NR2B versus NR2A transcripts in putative projection neurons (19), while dual-label in situ studies suggest a more balanced expression (39). Using the rapid immuno-LCM described, we report that striatal NOS-immunopositive interneurons are enriched in SOM mRNA (relative to NF-*l* chain mRNA), a chemical marker unique to this population of striatal neurons. By contrast, the relative expression of NR2A, NR2B, and IT15 mRNAs was marked-

ly less. A specific NR2D product was detected, which is consistent with the restricted expression of this mRNA in striatal interneurons (40), whereas a NR2C product was not detected, consistent with the lack of expression of this transcript in striatal neurons (39). Thus, our data are consistent with previous mRNA studies in that they confirm the very low levels of NR2A, NR2B, and NR2D mRNA present in striatal NOS neurons, in particular the ratio of 2:1 for NR2A:NR2B that was reported in a dual-label in situ hybridization study (39). The unexpected finding was the relative enrichment of NR1 transcripts expressed by this discrete population of NOS-immunopositive interneurons; whether this represents contamination of the NOS sample pool by the somata of adjacent striatal ENK mRNA containing projection neurons and/or mRNA contained within neighboring cellular processes (35) is unclear. Such contamination of the NOS sample pool is consistent across all three samples and clearly does not reflect sample contamination by glia, as GFAP mRNA and NR2C mRNA (glial markers) were not detected.

In summary, the use of rapid immuno-LCM in combination with real-time PCR provides a direct method for examining the expression profile of mRNAs in a discrete population of neurons laser-dissected from a heterogeneous tissue section. Currently, this technique is being applied to the quantitative analysis of diseased tissue to determine the cellular origin of transcriptional dysregulation in the brain of Huntington's disease transgenic mice. This method is readily adaptable to conduct focused or genome-wide analyses in virtually any neuronal population in the mammalian brain.

ACKNOWLEDGMENTS

These studies were supported by the Hereditary Disease Foundation and the Huntington's Disease Society of America (S.J.A.).

REFERENCES

1. **Alizadeh, A.A., M.B. Eisen, R.E. Davis, C. Ma, I.S. Lossos, A. Rosenwald, J.C. Boldrick, H. Sabet, et al.** 2000. Distinct types of diffuse large B-cell lymphoma identified by gene expression profiling. Nature *403*:503-511.
2. **Augood, S.J., E.M. McGowan, and P.C. Emson.** 1994. Expression of N-methyl-D-aspartate receptor subunit NR1 messenger RNA by identified striatal somatostatin cells. Neuroscience *59*:7-12.
3. **Beal, M.F., N.W. Kowall, D.W. Ellison, M.F. Mazurek, K.J. Swartz, and J.B. Martin.** 1986. Replication of the neurochemical characteristics of Huntington's disease by quinolinic acid. Nature *321*:168-171.
4. **Beal, M.F., N.W. Kowall, K.J. Swartz, and R.J. Ferrante.** 1990. Homocysteic acid lesions in rat striatum spare somatostatin-neuropeptide Y (NADPH-diaphorase) neurons. Neurosci. Lett. *108*:36-42.
5. **Beal, M.F., N.W. Kowall, K.J. Swartz, R.J. Ferrante, and J.B. Martin.** 1989. Differential sparing of somatostatin-neuropeptide Y and cholinergic neurons following striatal excitotoxin lesions. Synapse *3*:38-47.
6. **Bonaventure, P., H. Guo, B. Tian, X. Liu, A. Bittner, B. Roland, R. Salunga, X.J. Ma, et al.** 2002. Nuclei and subnuclei gene expression profiling in mammalian brain. Brain Res. *943*:38-47.
7. **Brouillet, E., P. Hantraye, R.J. Ferrante, R. Dolan, A. Leroy-Willig, N.W. Kowall, and M.F. Beal.** 1995. Chronic mitochondrial energy impairment produces selective striatal degeneration and abnormal choreiform movements in primates. Proc. Natl. Acad. Sci. USA *92*:7105-7109.
8. **Bustin, S.A.** 2000. Absolute quantification of mRNA using real-time reverse transcription polymerase chain reaction assays. J. Mol. Endocrinol. *25*:169-193.
9. **Colantuoni, C., A.E. Purcell, C.M. Bouton, and J. Pevsner.** 2000. High throughput analysis of gene expression in the human brain. J. Neurosci. Res. *59*:1-10.
10. **de Almeida, L.P., C.A. Ross, D. Zala, P. Aebischer, and N. Deglon.** 2002. Lentiviral-mediated delivery of mutant huntingtin in the striatum of rats induces a selective neuropathology modulated by polyglutamine repeat size, huntingtin expression levels, and protein length. J. Neurosci. *22*:3473-3483.
11. **Dolter, K.E. and J.C. Braman.** 2001. Small-sample total RNA purification: laser capture microdissection and cultured cell applications. BioTechniques *30*:1358-1361.
12. **Emmert-Buck, M.R., R.F. Bonner, P.D. Smith, R.F. Chuaqui, Z. Zhuang, S.R. Goldstein, R.A. Weiss, and L.A. Liotta.** 1996. Laser capture microdissection. Science *274*:998-1001.
13. **Fend, F., M.R. Emmert-Buck, R. Chuaqui, K. Cole, J. Lee, L.A. Liotta, and M. Raffeld.** 1999. Immuno-LCM: laser capture microdissection of immunostained frozen sections for mRNA analysis. Am. J. Pathol. *154*:61-66.
14. **Ferrante, R.J., N.W. Kowall, M.F. Beal, E.P. Richardson, Jr., E.D. Bird, and J.B. Martin.** 1985. Selective sparing of a class of striatal neurons in Huntington's disease. Science *230*:561-563.
15. **Ferrante, R.J., N.W. Kowall, P.B. Cipolloni, E. Storey, and M.F. Beal.** 1993. Excitotoxin lesions in primates as a model for Huntington's

disease: histopathologic and neurochemical characterization. Exp. Neurol. *119*:46-71.
16. **Fink, L., T. Kinfe, W. Seeger, L. Ermert, W. Kummer, and R.M. Bohle.** 2000. Immunostaining for cell picking and real-time mRNA quantitation. Am. J. Pathol. *157*:1459-1466.
17. **Fink, L., W. Seeger, L. Ermert, J. Hanze, U. Stahl, F. Grimminger, W. Kummer, and R.M. Bohle.** 1998. Real-time quantitative RT-PCR after laser-assisted cell picking. Nat. Med. *4*:1329-1333.
18. **Fusco, F.R., Q. Chen, W.J. Lamoreaux, G. Figueredo-Cardenas, Y. Jiao, J.A. Coffman, D.J. Surmeier, M.G. Honig, et al.** 1999. Cellular localization of huntingtin in striatal and cortical neurons in rats: lack of correlation with neuronal vulnerability in Huntington's disease. J. Neurosci. *19*:1189-1202.
19. **Ghasemzadeh, M.B., S. Sharma, D.J. Surmeier, J.H. Eberwine, and M.-F. Chesselet.** 1996. Multiplicity of glutamate receptor subunits in single striatal neurons: an RNA amplification study. Mol. Pharmacol. *49*:852-859.
20. **Gillespie, J.W., C.J. Best, V.E. Bichsel, K.A. Cole, S.F. Greenhut, S.M. Hewitt, M. Ahram, Y.B. Gathright, et al.** 2002. Evaluation of non-formalin tissue fixation for molecular profiling studies. Am. J. Pathol. *160*:449-457.
21. **Ginsberg, S.D., S.E. Hemby, V.M. Lee, J.H. Eberwine, and J.Q. Trojanowski.** 2000. Expression profile of transcripts in Alzheimer's disease tangle-bearing CA1 neurons. Ann. Neurol. *48*:77-87.
22. **Goldsworthy, S.M., P.S. Stockton, C.S. Trempus, J.F. Foley, and R.R. Maronpot.** 1999. Effects of fixation on RNA extraction and amplification from laser capture microdissected tissue. Mol. Carcinog. *25*:86-91.
23. **Henshaw, R., B.G. Jenkins, J.B. Schulz, R.J. Ferrante, N.W. Kowall, B.R. Rosen, and M.F. Beal.** 1994. Malonate produces striatal lesions by indirect NMDA receptor activation. Brain Res. *647*:161-166.
24. **Horii, A., P.F. Smith, and C.L. Darlington.** 2002. Application of real-time quantitative polymerase chain reaction to quantification of glutamate receptor gene expression in the vestibular brainstem and cerebellum. Brain Res. Brain Res. Protoc. *9*:77-83.
25. **Jones, M.B., H. Krutzsch, H. Shu, Y. Zhao, L.A. Liotta, E.C. Kohn, and E.F. Petricoin, 3rd.** 2002. Proteomic analysis and identification of new biomarkers and therapeutic targets for invasive ovarian cancer. Proteomics *2*:76-84.
26. **Karpuj, M.V., M.W. Becher, J.E. Springer, D. Chabas, S. Youssef, R. Pedotti, D. Mitchell, and L. Steinman.** 2002. Prolonged survival and decreased abnormal movements in transgenic model of Huntington disease, with administration of the transglutaminase inhibitor cystamine. Nat. Med. *8*:143-149.
27. **Kebelmann-Betzing, C., K. Seeger, S. Dragon, G. Schmitt, A. Moricke, T.A. Schild, G. Henze, and B. Beyermann.** 1998. Advantages of a new Taq DNA polymerase in multiplex PCR and time-release PCR. BioTechniques *24*:154-158.
28. **Kerner, J.A., D.G. Standaert, J.B. Penney, A.B. Young, and G.B. Landwehrmeyer.** 1998. Simultaneous isotopic and nonisotopic in situ hybridization histochemistry with cRNA probes. Brain Res Protocols *3*:22-32.
29. **Kurella, M., L.L. Hsiao, T. Yoshida, J.D. Randall, G. Chow, S.S. Sarang, R.V. Jensen, and S.R. Gullans.** 2001. DNA microarray analysis of complex biologic processes. J. Am. Soc. Nephrol. *12*:1072-1078.
30. **Luo, L., R.C. Salunga, H. Guo, A. Bittner, K.C. Joy, J.E. Galindo, H. Xiao, K.E. Rogers, et al.** 1999. Gene expression profiles of laser-captured adjacent neuronal subtypes. Nat. Med. *5*:117-122.
31. **Luthi-Carter, R., A. Strand, N.L. Peters, S.M. Solano, Z.R. Hollingsworth, A.S. Menon, A.S. Frey, B.S. Spektor, et al.** 2000. Decreased expression of striatal signaling genes in a mouse model of Huntington's disease. Hum. Mol. Genet. *9*:1259-1271.
32. **Mallard, E.C., H.J. Waldvogel, C.E. Williams, R.L.M. Faull, and P.D. Gluckman.** 1995. Repeated asphyxia causes loss of striatal projection neurons in the fetal sheep brain. Neuroscience *65*:827-836.
33. **Meade, C.A., G. Figueredo-Cardenas, F. Fusco, T.S. Nowak, Jr., W.A. Pulsinelli, and A. Reiner.** 2000. Transient global ischemia in rats yields striatal projection neuron and interneuron loss resembling that in Huntington's disease. Exp. Neurol. *166*:307-323.
34. **Mishra, O.P., K.I. Fritz, and M. Delivoria-Papadopoulos.** 2001. NMDA receptor and neonatal hypoxic brain injury. Ment. Retard. Dev. Disabil. Res. Rev. *7*:249-253.
35. **Mohr, E.** 1999. Subcellular RNA compartmentalization. Prog. Neurobiol. *57*:507-525.
36. **Norris, P., H. Waldvogel, R. Faull, D. Love, and P. Emson.** 1996. Decreased neuronal nitric oxide synthase messenger RNA and somatostatin messenger RNA in the striatum of Huntington's disease. Neuroscience *72*:1037-1047.
37. **Rekhter, M.D. and J. Chen.** 2001. Molecular analysis of complex tissues is facilitated by laser capture microdissection: critical role of upstream tissue processing. Cell Biochem. Biophys. *35*:103-113.
38. **Salunga, R., H. Guo, L. Luo, A. Bittner, K. Joy, J. Chambers, J. Wan, M. Jackson, and M. Erlander.** 1999. Gene expression analysis via cDNA microarrays of laser capture microdissected cells from fixed tissue, p. 121-137. *In* M. Schena (Ed.), DNA Microarrays. Oxford University Press.
39. **Standaert, D., I. Friberg, G. Landwehrmeyer, A. Young, and J. Penney.** 1999. Expression of NMDA receptor subunit mRNAs in neurochemically identified projection and interneurons in the striatum of the rat. Mol. Brain Res. *64*:11-23.
40. **Standaert, D.G., G.B. Landwehrmeyer, J.A. Kerner, J.B. Penney, and A.B. Young.** 1996. Expression of NMDAR2D glutamate receptor subunit mRNA in neurochemically identified interneurons in the rat neostriatum, neocortex and hippocampus. Mol. Brain Res. *42*:89-102.
41. **Surmeier, J.D., W.-J. Song, and Z. Yan.** 1996. Coordinated expression of dopamine receptors in neostriatal medium spiny neurons. J. Neurosci. *16*:6579-6591.
42. **Trogan, E., R.P. Choudhury, H.M. Dansky, J.X. Rong, J.L. Breslow, and E.A. Fisher.** 2002. Laser capture microdissection analysis of gene expression in macrophages from atherosclerotic lesions of apolipoprotein E-deficient mice. Proc. Natl. Acad. Sci. USA *99*:2234-2239.
43. **Vincent, S.R. and O. Johansson.** 1983. Striatal neurons containing both somatostatin- and avian pancreatic polypeptide (APP)-like immunoreactivities and NADPH-diaphorase activity: a light and electron microscopic study. J. Comp. Neurol. *217*:264-270.
44. **Walch, A., K. Specht, J. Smida, M. Aubele, H. Zitzelsberger, H. Hofler, and M. Werner.** 2001. Tissue microdissection techniques in quantitative genome and gene expression analyses. Histochem. Cell Biol. *115*:269-276.
45. **Wulfkuhle, J.D., K.C. McLean, C.P. Paweletz, D.C. Sgroi, B.J. Trock, P.S. Steeg, and E.F. Petricoin, 3rd.** 2001. New approaches to proteomic analysis of breast cancer. Proteomics *1*:1205-1215.

Received 18 July 2002; accepted 29 August 2002.

Address correspondence to:

Dr. Sarah J. Augood
Department of Neurology
Center for Aging, Genetics and Neurodegeneration
Massachusetts General Hospital
114 16th Street
Charlestown, MA 20129, USA
e-mail: augood@helix.mgh.harvard.edu